V International Conference on Particle-based Methods – Fundamentals and Applications
PARTICLES 2017
P. Wriggers, M. Bischoff, E. Oñate, D.R.J. Owen, & T. Zohdi (Eds)

INVESTIGATIONS OF QUASI-STATIC VORTEX-STRUCTURES IN 3D SAND SPECIMENS BASED ON DEM AND HELMHOLTZ-HODGE VECTOR FIELD DECOMPOSITION

J. KOZICKI[1] AND J. TEJCHMAN[2]

[1]Gdansk University of Technology
80-233 Gdansk, Narutowicza 11/12
jkozicki@pg.gda.pl

[2]Gdansk University of Technology
80-233 Gdansk, Narutowicza 11/12
tejchmk@pg.gda.pl

Key words: Granular Materials, Plane strain compression, DEM, Helmholtz-Hodge decomposition, Vortex-structures.

Abstract. The paper presents some three-dimensional simulation results of granular vortex-structures in cohesionless initially dense sand during quasi-static plane strain compression. The sand behaviour was simulated using the discrete element method (DEM). Sand grains were modelled by spheres with contact moments to approximately capture the irregular grain shape. The Helmholtz-Hodge decomposition (HHD) of the displacement vector field from DEM calculations was used. The variational discrete multiscale vector field decomposition allowed for separating a vector field into the sum of three uniquely defined components: curl free, divergence free and harmonic. Vortex-structures were strongly connected to shear localization. They slightly changed along the specimen depth. They localized in locations where shear zones ultimately developed.

1 INTRODUCTION

Granular vortex-structures defined as the roughly swirling (rotating) motion of several grains around a common central point were frequently observed in experiments on granular materials [1]-[3] and in calculations using the discrete element method (DEM) [4]-[9]. They became apparent in experiments and calculations when the motion associated with uniform (affine) strain was subtracted from the actual granular deformation. They are reminiscent of turbulence in fluid dynamics, however the amount of the grain rotation is several ranges of magnitude smaller (~0.01^o-0.1^o) than the fluid vortex rotation, their life time is also short than of eddies in turbulent fluid flow and granular flow is too slow to induce inertial forces characteristic for turbulences in fluid. The vortices have been mainly observed in shear zones that are the fundamental phenomenon in granular bodies. A dominant mechanism responsible for the vortex formation was the breakage of force chains [4], [7]. The collapse of main force chains lead to a formation of larger voids and their build-up to a formation of smaller voids [7]. Kozicki and Tejchman [8], [9] and Tordesillas et al. [4] showed that shear localization may be predicted very early through vortex-structures that means new perspectives for a

detection of impending failure in granular bodies (inherently connected with shear localization) within continuum mechanics. In continuous and discontinuous numerical calculations and laboratory experiments, shear localization is usually identified in granular bodies by grain rotations or micro-polar rotations or by an increase of void ratio.

The aim of the present paper is to present the results of 3D vortex-structures in sand during quasi-static plane strain compression by using the Helmholtz-Hodge decomposition (HHD) of a vector field [10], [11] calculated by the discrete element method (DEM) [8]. Attention was paid to the relationship between vortex-structures and shear localization with respect to the location and formation moment. The analyses were carried out with spheres with contact moments to approximately capture the irregular grain shape. In order to accelerate the computation time, some simplifications were assumed in analyses: large spheres with contact moments, linear sphere distribution, linear normal contact model and no particle breakage. A three-dimensional discrete model YADE developed at University of Grenoble by Donze and his co-workers was applied [12], [13]. The discrete calculations were solely carried out with initially dense sand. The innovative point of our calculations are 3D granular vortex-structures which have not been calculated in granular materials yet.

In our previous paper we calculated 2D vortex-structures during a quasi-static passive wall translation based on the Helmholtz-Hodge decomposition (HHD) of a vector field calculated by the discrete element method (DEM) [9]. The discrete vector field decomposition proved to be an objective, universal and effective technique for identifying all 2D vortex-structures during granular flow which was directly based on single grain displacement increments (but not on displacement fluctuations). The method did not use any additional non-objective parameters. However the method did not determine the size of vortex-structures. A strong connection between the location of vortex-structures and progressive shear localization was found out. The vortex-structures were the precursor of shear localization since they clearly concentrated in the area where shear zones ultimately later formed. Thus the ultimate shear zone pattern was detected in early loading stages. The vortex-structures allowed to identify shear localization significantly earlier than e.g. based on single grain rotations which were always a reliable indicator of shear localization. They developed from the deformation process beginning. They solely emerged in main shear zones. They had a tendency to move along shear zones. Their number varied and was larger on average at the residual state. The right-handed vortices were dominant in the curved shear zone and left-handed ones were dominant in the radial shear zone. In the curved shear zone, the predominant period of right-handed vortices was 4% of u/h during the entire wall movement. In the radial shear zone, the predominant period of left-handed vortices was also 4% of u/h. In the residual state, local regions of dilatacy and contractancy alternately happened along globally dilatant shear zones with a dominance of local dilatancy.

2 THREE-DIMENSIONAL DEM MODEL

In order to simulate the behaviour of real sand, the 3D explicit spherical discrete element model YADE, developed at University of Grenoble [12]-[13]. DEM includes the simple mathematical treatment of engineering problems (complex global constitutive relationships are replaced by simple local contact laws) and has the natural predisposition to account for material heterogeneity. The outstanding advantages of DEM include its ability to explicitly

handle the discrete/heterogeneous nature of the material by modelling particle-scale properties including size and shape which play an important role in shear localization. The disadvantages is an enormous computational cost and an extensive calibration based on experimentally measured macro-scale properties. The algorithm used in the present DEM which is based on a description of particle interactions in terms of force laws involves in general main steps [14]. First, based on constitutive laws, interaction forces between discrete elements are computed. Second, the Newton's second law is applied to determine for each element the resulting acceleration, which is then time integrated to find the new position. This process is repeated until the simulation is finished. The method takes advantage of the so-called soft-particle approach, i.e. the model allows for particle deformation which is modelled as an overlap of particles. During the simulations, particles may overlap that can be interpreted as a local contact deformation. A linear elastic normal contact model was used only. In compression, the normal force was not restricted and could increase indefinitely. The interaction forces acting on each element in the form of normal and tangential forces were linked to the displacements through the normal stiffness K_n and tangential stiffness K_s

$$\vec{F}_n = K_n U \vec{N}, \tag{1}$$

$$\vec{F}_s = \vec{F}_s + \Delta\vec{F}_s \qquad \text{with} \qquad \Delta\vec{F}_s = K_s \Delta\vec{X}_s, \tag{2}$$

where U is the penetration depth between discrete elements, $\vec{N}$ denotes the unit normal vector at the contact point and $\Delta\vec{X}_s$ is the incremental tangential displacement vector. The unloading was assumed to be purely elastic. The stiffness parameters were calculated in terms of the modulus of elasticity of the grain contact E_c and two contacting grain radii R_A and R_B (to determine the normal stiffness K_n) and in terms of the modulus of elasticity E_c and Poisson's ratio υ_c of the grain contact, and grain radii R_A and R_B (to determine the tangential stiffness K_s) of two contacting spheres, respectively [12]

$$K_n = E_c \frac{2R_A R_B}{R_A + R_B} \qquad \text{and} \qquad K_s = \nu_c E_c \frac{2R_A R_B}{R_A + R_B}. \qquad , \tag{3}$$

If the grain radius $R_A=R_B=R$, the stiffness parameters are equal to: $K_n=E_c\ R$ and $K_s=\upsilon_c\ E_c\ R$ (thus $K_s/K_n=\upsilon_c$), respectively. The frictional sliding starts at the contact point when the contact forces $\vec{F}_s$ and $\vec{F}_n$ satisfy the limit Coulomb condition

$$\left\|\vec{F}_s\right\| - \left\|\vec{F}_n\right\| \times \tan\mu \le 0 \tag{4}$$

with μ as the inter-particle friction angle (tension was not allowed). No forces are transmitted when grains are separated. The elastic contact constants were specified from the experimental data of a triaxial compression sand test and could be related to the modulus of elasticity of grain material E and its Poisson ratio ν [15], [16].

In order to increase the rolling resistance of pure spheres, clusters of spheres or contact moments were introduced. The normal force was assumed to contribute to the rolling

resistance. The contact moment increments were calculated by means of the rolling stiffness K_r multiplied by the angular rotational increment vectors $\Delta\vec{\omega}$

$$\Delta M = K_r \Delta\vec{\omega}\,. \tag{5}$$

The rolling stiffness K_r [kNm] in Eq.5 was related to the tangential stiffness K_s [kN/m] in Eq.2 by the following formula

$$K_r = \beta \times K_s \times R^2 = \beta \times K_s \times R_A R_B\,, \tag{6}$$

where β is the dimensionless rolling stiffness coefficient and R is the equivalent grain radius (at small displacements $dX_r \approx dX_s$). The dimensionless rolling coefficient η specifies the limit friction moment of the rolling motion [12]

$$|\vec{M}| - \eta \frac{R_A + R_B}{2} |\vec{F}_n| \le 0\,. \tag{7}$$

Because the proposed DEM is a fully dynamic formulation, a local non-viscous damping scheme was applied [14] in order to dissipate excessive kinetic energy in a discrete system and facilitate convergence towards quasi-static equilibrium. The damping parameter α was introduced to reduce contact forces and moments acting on elements

$$\vec{F}^k_{damped} = \vec{F}^k - \alpha \cdot \mathrm{sgn}(\vec{v}^k)\,|\vec{F}^k| \quad \text{and} \quad \vec{M}^k_{damped} = \vec{M}^k - \alpha \cdot \mathrm{sgn}(\vec{\omega}^k)\,|\vec{M}^k|\,, \tag{8}$$

where $\vec{F}^k$ and $\vec{M}^k$ are the k^{th} components of the residual force and moment vector and $\vec{v}^k$ and $\vec{\omega}^k$ are the k^{th} components of the translational and rotational velocity. A positive damping coefficient α is smaller than 1 (sgn(•) returns the sign of the k^{th} component of velocity). The equations are separately applied to each k-th component of a 3D vector x, y and z. The effect of damping is insignificant in quasi-static calculations [15], [16].

The five main local material parameters are necessary in our DEM simulations: E_c (modulus of elasticity of the grain contact), ν_c (Poisson's ratio of the grain contact), μ (inter-particle friction angle), β (rolling stiffness coefficient) and η (limit rolling coefficient). In addition, a particle radius R, particle mass density ρ and numerical damping parameter α are required. The DEM material parameters: E_c, ν_c, μ, β, η and α were calibrated using the corresponding homogeneous axisymmetric triaxial laboratory test results on Karlsruhe sand with the different initial void ratio and lateral pressure by Wu [17]. The procedure for determining the material parameters in DEM was described in detail by Kozicki et al. [15], [16]. The index properties of Karlsruhe sand are: mean grain diameter d_{50}=0.50 mm, grain size between 0.08 mm and 1.8 mm, uniformity coefficient U_c=2, maximum specific weight γ_d^{max}=17.4 kN/m^3, minimum void ratio e_{min}=0.53, minimum specific weight γ_d^{min}=14.6 kN/m^3

and maximum void ratio e_{max}=0.84. The sand grains are classified as sub-rounded/sub-angular. The following material constants were found in DEM by fitting numerical outcomes with experimental ones during homogeneous triaxial compression: E_c=0.3 GPa, ν_c=0.3, μ=18^o, β=0.7, η=0.4 ρ=2.55 g/cm^3 and a=0.08.

3 DEM RESULTS OF PLANE STRAIN COMPRESSION

Our numerical outcomes with respect to 3D vortex-structures were related quasi-static plane strain compression. The results of 3D DEM calculations were described in detail in [8]. The granular specimen used in DEM had the same size as in the experiments by Vardoulakis [18], namely: the width b=4 cm, height h=14 cm and depth l=8 cm (out-of-plane direction) (Fig.2). The linear grain distribution curve was assumed; the grain diameter range was between 1.25 mm and 3.75 mm with d_{50}=2.5 mm. About 56'000 spheres were used with the same material constants. The initial void ratio was e_o=0.53. The flexible vertical walls were assumed to model the membrane surrounding the specimen in experiments (Figs.2a and 2b). Both the front and rear specimen sides 4×14 cm^2 were blocked in a perpendicular direction to the specimen to enforce plane strain conditions. The bottom surface 4×8 cm^2 was fixed in a vertical direction and the top surface 4×8 cm^2 was subjected to the constant vertical displacement u_1. Along the top, bottom and membrane granular surfaces, the inter-particle friction angle was μ=0. During the loading process, the constant confining pressure of σ_c=200 kPa was applied through the flexible membrane.

Figure 2 demonstrates the typical evolution of the mobilized internal friction angle (calculated with principal stresses from the Mohr's equation) versus the vertical normal strain $\varepsilon_1=u_1/h$ and volumetric strain ε_v versus ε_1 for two specimens. Figure 3 shows the distribution of sphere rotations ω and void ratio e in the vertical mid-section slice with the area of 4×14 cm^2 and thickness of 5×d_{50} (1.25 cm, d_{50}=2.5 mm) cut out from the granular specimen 4×14×8 cm^3. The both quantities were calculated from the volumetric cell V_c=5d_{50}×5d_{50}×5d_{50} moved by d_{50} in two directions within the slice to create a 2D grid of the averaged values from the cell. The cell size, which was smaller than the shear zone thickness t_s, was chosen with preliminary calculations. The averaging cell larger than V_c caused the results too diffusive and with the smaller cell volume V_c, the results started too strongly fluctuate.

Similarly as in real experiments [18], the initially dense specimen showed an asymptotic behaviour; it exhibited initially small elasticity, hardening (connected first to contractancy and then dilatancy), reached a peak of ϕ_{max}=46^o at about of ε_1=5%, gradually softened and dilated reaching a residual state of ϕ_{max}=30^o at the large vertical strain of 25-30% (Fig.3). The coordination number was initially about 5 and decreased down next to 3.8 during shearing due to dilatancy. During deformation a distinct internal inclined shear zone occurred inside the sand specimen which was marked by shear strain, larger grain rotation and volume increase (Fig.3). The thickness of the inclined interior shear zone t_s was on average in the residual state for ε_1=30% about t_s=25 mm (10×d_{50}) based on strain deformation in the specimen. The calculated shear zone inclination to the bottom was 60^o at ε_1=10% and 67^o at ε_1=30%.. In the calculated shear zone, the mean void ratio and grain rotation were: e>0.65 and ω>25^o. The specimen globally dilated in the shear zone. At the critical state, the maximum average void ratio was 0.70-0.80 in the shear zone and 0.53-0.60 outside. The maximum resultant rotation in the shear zone at the peak (ε_1=5%) was about ω=5^o and at the residual

state for ε_1=30% between ω=50°-55°. Based on both the cumulative rotation and void ratio (Fig.3), the internal inclined shear zone may be noticed for $\varepsilon_1 \geq 5\%$.

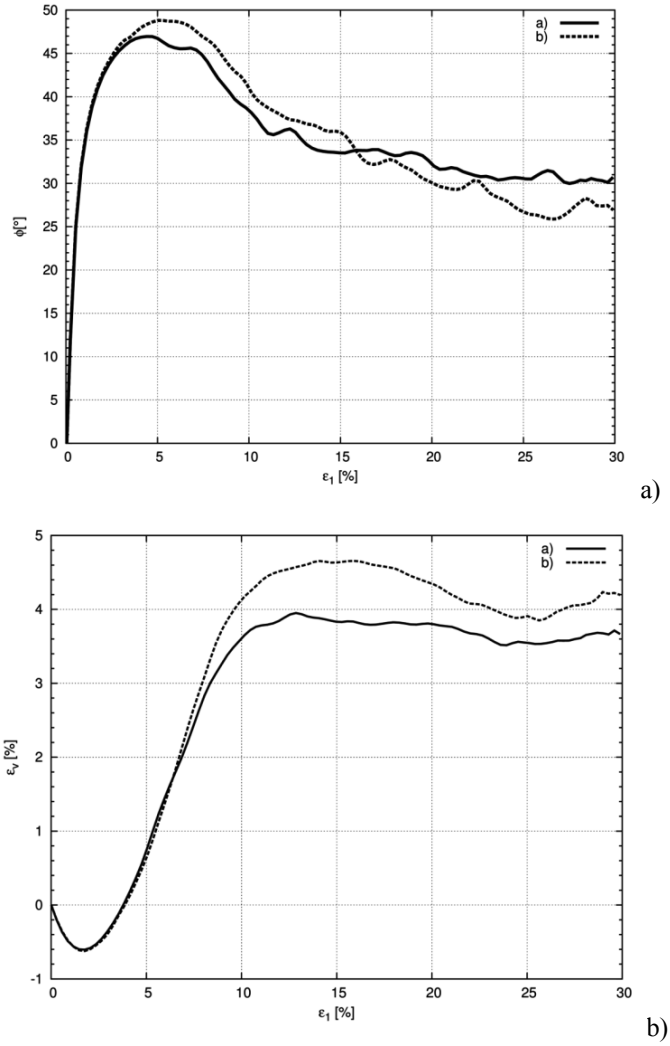

Figure 2: DEM results for plane strain compression with initially dense sand (e_o=0.53, σ_c=200 kPa, d_{50}=2.5 mm, E_c=0.3 GPa, ν_c=0.3, μ=18°, β=0.7, η=0.4) for two simulations: a) mobilized internal friction angle ϕ versus normalized vertical displacement of specimen top $\varepsilon_1=u_1/h$ and b) volumetric strain ε_v versus ε_1 (h - initial specimen height) [8]

4 HELMHOLTZ-HODGE DECOMPOSITION (HHD)

4.1 Calculation's method

The Helmholtz-Hodge decomposition (HHD) of vector fields is one of the fundamental theorems in fluid dynamics [10], [11], [19]. It describes a vector displacement increment field in terms of its curl-free and divergence-free components based on potential functions. The unique Helmholz-Hodge decomposition of the smooth 3D vector field $\vec{\xi}$ provides the following formula

$$\vec{\xi} = \vec{\nabla} u + \vec{\nabla} \times \vec{v} + \vec{h}, \tag{10}$$

where $\nabla = \left(\frac{\partial}{\partial x}, \frac{\partial}{\partial y}, \frac{\partial}{\partial z}\right)^T$ is the gradient, $\nabla \cdot = \left(\frac{\partial}{\partial x} + \frac{\partial}{\partial y} + \frac{\partial}{\partial z}\right)$ denotes the divergence operator, $\nabla \times$ is the curl operator, u denotes the scalar potential field, $\vec{v}$ is the vector potential field and $\vec{h}$ denotes the harmonic vector field. The gradient of the scalar potential function $\vec{\nabla} u$ is called the curl-free component and is related to expansion/contraction (because is irrotational) while the curl of the vector potential function $\vec{\nabla} \times \vec{v}$ is called the divergence-free component and is related to vorticity and pure shear (because is incompressible). The harmonic component which contains the non-integrable component of the field, is related to pure translation.

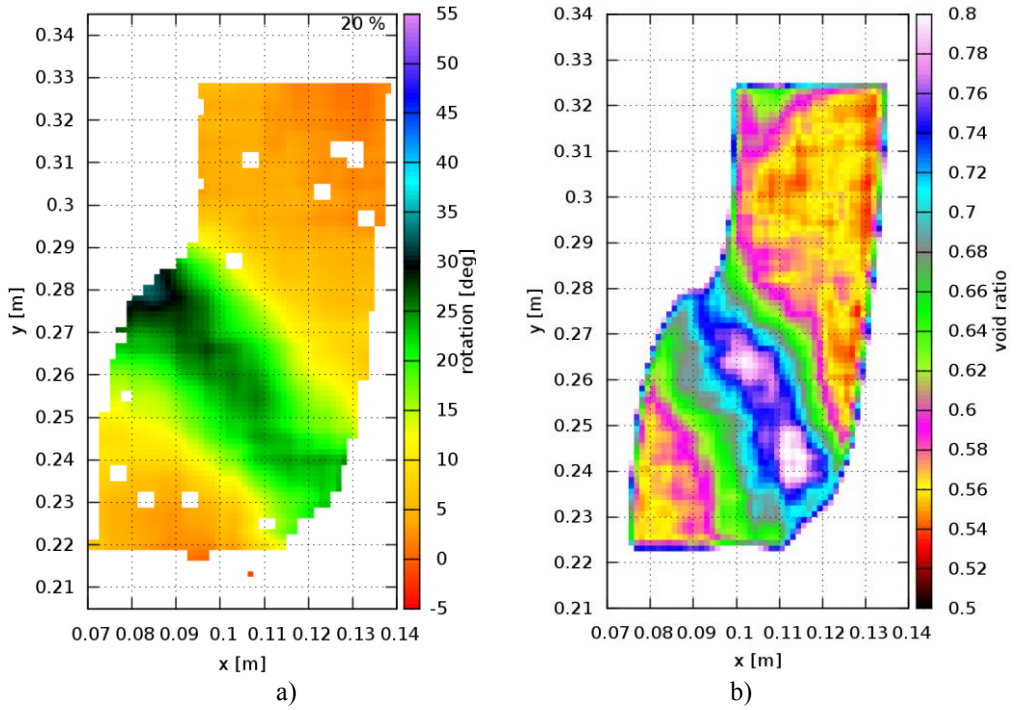

Figure 3: DEM results for plane strain compression test with initially dense sand (e_o=0.53, σ_c=200 kPa, d_{50}=2.5 mm): average cumulative grain rotation distribution and average cumulative void ratio distribution in degrees in granular specimen for vertical normal strain ε_l=20% [8]

A variational calculus approach was used [20] which allowed for finding the vector fields $\vec{\nabla} u$ and $\vec{\nabla} \times \vec{v}$ by examining the difference between the unknown vector field and provided field $\vec{\xi}$. By requesting that this difference is minimum (the minimum was found by assuming that the derivatives of the functionals were equal to zero, the vector fields $\vec{\nabla} u$ and $\vec{\nabla} \times \vec{v}$ were explicitly determined. The explicit calculation for $\vec{\nabla} u$ and $\vec{\nabla} \times \vec{v}$ was given in [9].

The accurate discrete multiscale Helmholz-Hodge decomposition of vector fields on arbitrary tetrahedral grids was proposed in [19]. In order to create a grid, the centre of each sphere was a node in the Delaunay triangulation and the i-th node had the coordinate $\vec{r}_i$. Then

the discrete piecewise-constant vector field $\vec{\xi}(\vec{r}_i) = \sum_k \psi_k(\vec{r})\,\overrightarrow{\xi_k}$ was created by assigning the constant vector value $\overrightarrow{\xi_k}$ to each k-th tetrahedron (ψ_k is the piecewise-constant basis function equal to 1 inside the k-th tetrahedron and 0 otherwise). This value was calculated as the average of sphere displacement increments $\overrightarrow{d_n}$ which constituted each tetrahedron $\overrightarrow{\xi_k} = 1/4 \sum_{n=1}^{n=4} \overrightarrow{d_n}$ in the 3D case or each triangle $\overrightarrow{\xi_k} = 1/3 \sum_{n=1}^{n=3} \overrightarrow{d_n}$ in the 2D case. Since u and $\vec{v}$ are the piecewise linear functions described using a piecewise-linear basis shape function $\phi_i(\vec{r})$, their derivatives ∇ will be piecewise-constant, hence the solution for the piecewise-constant $\vec{\xi}(\vec{r})$ discrete vector field is exact [19].

4.2 Boundary conditions

In order to obtain a unique solution, appropriate boundary conditions have to be assumed [11], [21]. The system of linear equations in HHD was solved using the following general boundary conditions: $\vec{\nabla} \times \vec{v}$ (divergence-free component - incompressible component) was tangential to the domain boundary $\vec{v}|_{\partial T}$=0 and $\vec{\nabla} u$ (curl-free component - irrotational component) was orthogonal to the boundary domain $u|_{\partial T}$=0. The proof of uniqueness and orthogonality for these boundary conditions, called N-P (normal-parallel) boundary conditions, which should be always maintained for flow problems can be found in [22]. Note that a change of these boundary conditions suggested in [23] may create an invalid or ill-posed problem [24]. The so-called Hodge-Morrey-Friedrichs boundary conditions may be also used [11]. The boundary conditions obviously influence vector fields close to specimen boundaries. In particular when the spheres' number is low; vortex-structures may be solely detected in the specimen centre since the vector field $\vec{\nabla} \times \vec{v}$ is forced by boundary conditions to be parallel to boundaries. In our previous calculations [9] the number of spheres along the height and length of the granular specimen was high enough (200-400) and the effect of boundaries proved to be insignificant on the distribution of vortices based on preliminary calculations. Due to a rather small number of particles along the specimen width during plane strain compression (≈16=b/d_{50}=40/2.5), the effect of boundary conditions during calculations of vortex-structures was weakened by introducing virtual particles outside boundaries [22]. Artificial nodes were added in the Delaunay's triangular mesh at the distance of up to 50 mm around the specimen (with the grid inter-node distance of 1 mm).The vector $\vec{\xi}$ in these artificial nodes was calculated using the Gaussian averaging for true specimen nodes with the averaging radius of 80 mm (2×b).

5 NUMERICAL RESULTS

Figures 4 and 5 show the calculated 3D vortex-structures in the granular specimens. The spatial view on the net of vortex-structures is shown in Fig.4 (the vortex-structures are shown in the form of cylinders which linked all local maxima). Figure 5 presents the vortex-structures at 3 different vertical cross-sections (specimen front side, specimen mid-depth and specimen rear side) for 5 different vertical normal strains ε_1: ε_1=1.5%, ε_1=3%, ε_1=5%, ε_1=10% and ε_1=20%. The circles denote the spots where the vertical cross-sections intersected the 3D vortex lines of Fig.4.

The vortex-structures appeared from the begin of the specimen deformation. They were immediately concentrated in the region of the shear zone occurrence. Thus the ultimate shear zone turned out to be encoded in the grain kinematics from the deformation onset. This outcome is in accordance with our earlier calculation results for plane strain compression based on displacement fluctuations [8] and calculation results based on bottlenecks in force transmission through the contact network [24]. The right-handed vortices (green circles) were created during progressive deformation. The distribution of vortex-structures was not uniform in the specimen and their number was different in vertical cross-sections up to the residual state. The number of vortex-structure was smaller in 3D simulations than in 2D ones.

6 CONCLUSIONS

- The vortex-structures were the precursor of shear localization since they clearly concentrated in the area where a shear zone ultimately later formed. Thus the ultimate shear zone was detected in early loading stages. The vortex-structures allowed to identify shear localization significantly earlier than e.g. based on single grain rotations or an increase of void ratio which were always a reliable indicator of shear localization. They developed from the deformation process beginning.
- An early prediction possibility of shear localization through vortex-structures may open new perspectives for a detection of impending failure in granular bodies (inherently connected with shear localization) within continuum mechanics.

ACKNOWLEDGMENT

The authors would like to acknowledge the support by the grant 2011/03/B/ST8/05865 "*Experimental and theoretical investigations of micro-structural phenomena inside of shear localization in granular materials*" financed by the Polish National Science Centre.

REFERENCES

[1] Utter, B. and Behringer, RP. Self-diffusion in dense granular shear flows. *Phys. Rev. E*. (2004) **69** (3), 031308-1–031308-12.
[2] Abedi, S., Rechenmacher A.L. and Orlando A.D. Vortex formation and dissolution in sheared sands. *Granular Matter* (2012) **14**: 695-705.
[3] Richefeu, V., Combe, G. and Viggiani G. An experimental assessment of displacement fluctuations in a 2D granular material subjected to shear. *Geotechnique Letters* (2012) **2**:113-118.
[4] Tordesillas, A., Pucilowski, S., Lin, Q., Peters, J.F. and Behringer, RP. Granular vortices: identification, characterization and conditions for the localization of deformation. *Journal of Mechanics and Physics of Solids* (2016) **90**: 215-241.
[5] Peters, J.F. and Walizer, L.E. Patterned non-affine motion in granular media**.** *Journal of Engineering Mechanics* (2013) **139** (10): 1479-1490.
[6] Nitka M, Tejchman J. Modelling of concrete behaviour in uniaxial compression and tension with DEM. *Granular Matter* 2014, 17 (1), 145-164.
[7] Nitka M, Tejchman J, Kozicki J, Leśniewska D. DEM analysis of micro-structural events within granular shear zones under passive earth pressure conditions. *Granular Matter* 2015, 3, 325-343.

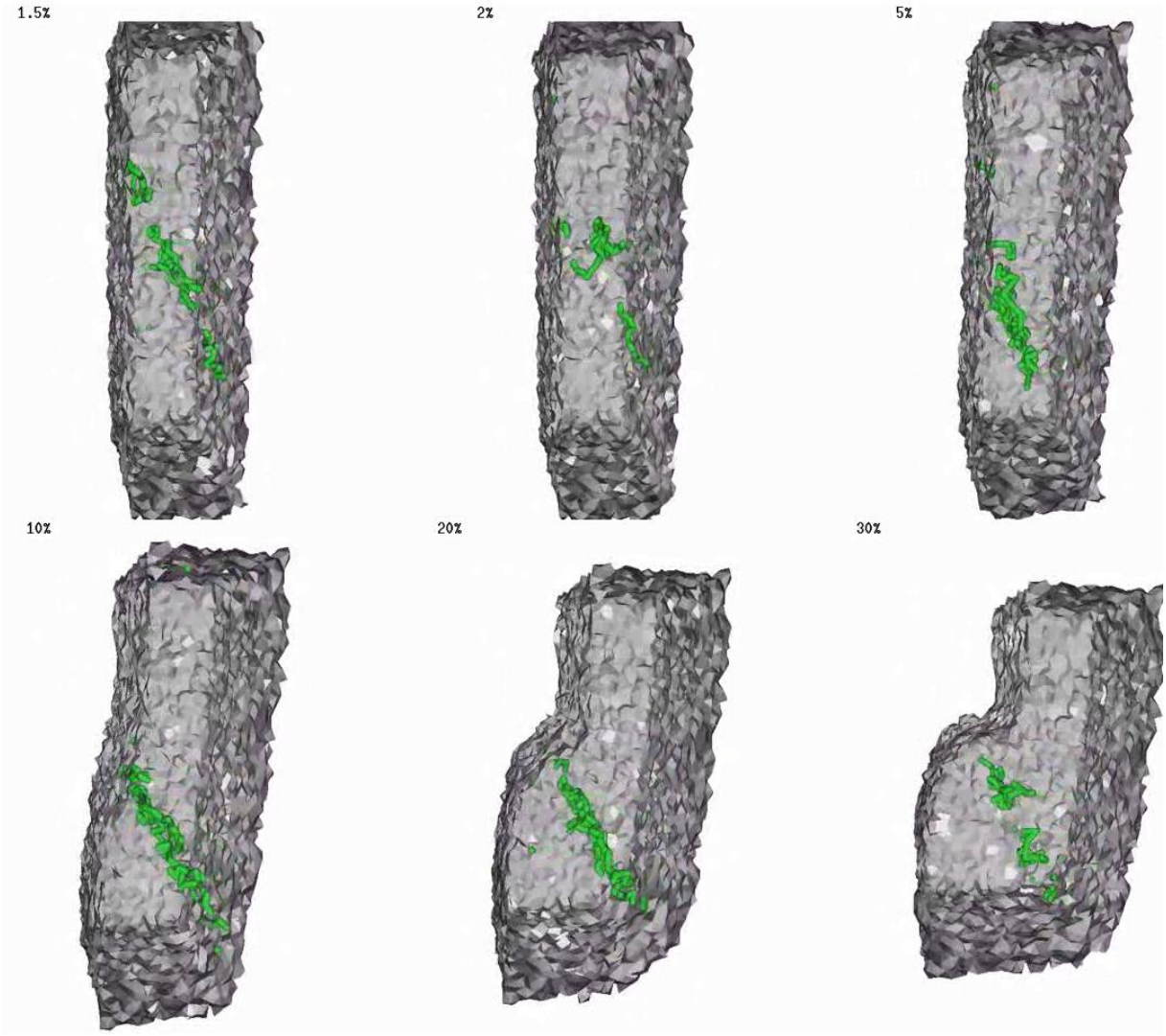

Figure 4: 3D vortex-structures in 3 for different vertical normal strain ε_l=1.5%-30% (green lines link local minima (right-handed vortices)

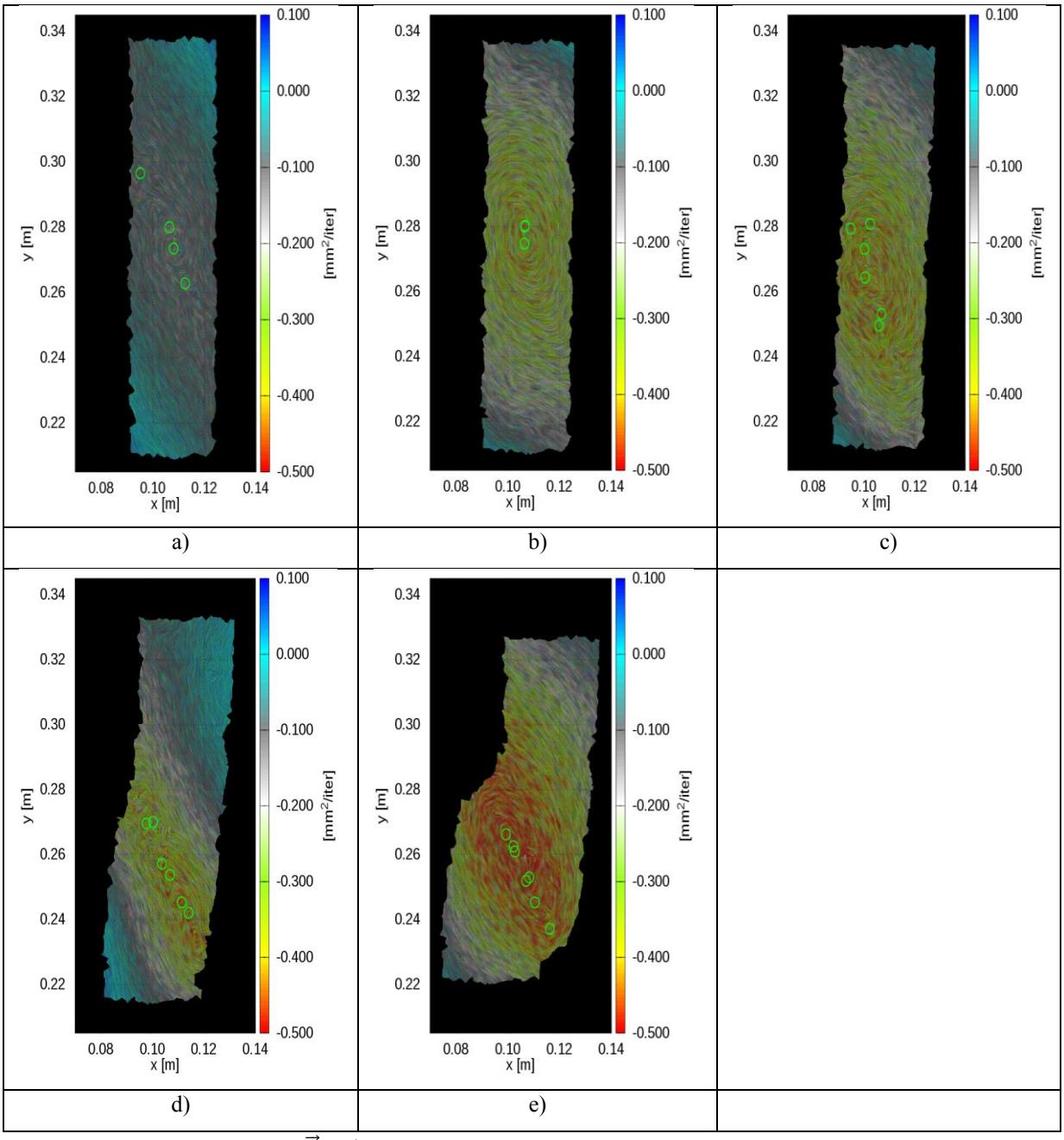

Figure 5: 3D vector field curl $\vec{\nabla} \times \vec{v}$ (divergence-free component related to vorticity) in granular specimen area $x \times y$ in vertical cross-section at specimen mid-depth for different vertical normal strain ε_1: a) ε_1=1.5%, b) ε_1=3%, c) ε_1=5%, d) ε_1=10% and e) ε_1=20%, (scale denotes component of vector potential $\vec{v}$ perpendicular to specimen in [mm^2/iteration]), green circles describe local minima (right-handed vortices))

[8] Kozicki, J. and Tejchman, J. DEM investigations of two-dimensional granular vortex- and anti-vortex- structures during plane strain compression. *Granular Matter* (2016) **2**, 20: 1-28.
[9] Kozicki J, Tejchman J. Investigations of quasi-static vortex structures in 2D sand specimen under passive earth pressure conditions based on DEM and Helmholtz-Hodge vector field decomposition. *Granular Matter* (2017) **19** (2), 19-31.
[10] Helmholtz H. Über Integrale der Hydrodynamischen Gleichungen, Welche den Wirbelbewegungen Entsprechen. (German) *J. für die Reine und Angewandte Mathematik* (1858) **55**: 25-55.
[11] Bhatia, H. and Pascucci, V. The Helmholtz-Hodge decomposition - a survey. *IEEE Transactions on Visualization and Computer Graphics* (2013), **19** (8): 1386-1404.
[12] Kozicki, J. and Donze, F.V. A new open-source software developed for numerical simulations using discrete modelling methods. *Computer Methods in Applied Mechanics and Engineering* (2008) **197**: 4429-4443.
[13] Šmilauer, V. and Chareyre, B. *Yade DEM Formulation*. Manual (2011).
[14] Cundall, P.A. and Strack, O.D.L. A discrete numerical model for granular assemblies. *Geotechnique* (1979) **29**: 47-65.
[15] Kozicki, J., Tejchman, J. and Mróz, Z. Effect of grain roughness on strength, volume changes, elastic and dissipated energies during quasi-static homogeneous triaxial compression using DEM. *Granular Matter* (2012) **14**(4):457-468.
[16] Kozicki, J., Tejchman J. and Műhlhaus, H.B. Discrete simulations of a triaxial compression test for sand by DEM. *Int. J. Num. Anal. Methods in Geomech.* (2014) **38**: 1923-1952.
[17] Wu, W. Hypoplastizität als mathematisches Modell zum mechanischen Verhalten granularer Stoffe. *Heft 129, Institute for Soil- and Rock-Mechanics, University of Karlsruhe*, 1992.
[18] Vardoulakis, I. Shear band inclination and shear modulus in biaxial tests. *Int. J. Numer. Anal. Methods Geomech*. (1980) **4**: 103-119.
[19] Tong, Y, Lombeyda, S, Hirani, A.N. and Desbrun, M. Discrete multiscale vector field decomposition. *ACM Transactions on Graphics* (TOG) (2003) 22 (3): 445-452.
[20] Gelfand, I.M. and Fomin, S.V. Calculus of variations. Dover Publications INC, Mineola, New York, 1963 (re-published in 2001), ISBN 9780486414485.
[21] Denaro, F.M. On the application of the helmholtz-hodge decomposition in projection methods for incompressible flows with general boundary conditions. *Int. J. Numerical Methods in Fluid*s (2003) **43**: 43-69.
[22] Petroneto, F., Paiva, A., Lage, M., Tavares, G., Lopes, H. and Lewiner, T. Meshless Helmholz-Hodge decomposition. *IEEE Transactions on Visualization and Computer Graphics* 2010, **16**: 338-349.
[23] Bhatia, H., Norgard, G., Pascucci, V. and Bremer, P.T. Comments on the meshless helmholtz-hodge decomposition. IEEE Transactions on Visualization and Computer Graphics (2013) **19** (3): 527-529.
[24] Tordesillas A, Pucilowski S, Tobin S, Kuhn M, Ando E, Viggiani G, Druckrey A. and Alshibli K. Shear bands as bottlenecks in force transmission. *EPL* (2015) **110**: 58005.

3 TITLE, AUTHORS, AFFILIATION, KEY WORDS

The first page must contain the Title, Author(s), Affiliation(s), Key words and the Summary. The Introduction must begin immediately below, following the format of this template.

3.1 Title

The title should be written centered, in 14pt, boldface Roman, all capital letters. It should be single spaced if the title is more than one line long.

3.2 Author

The author's name should include first name, middle initial and surname. It should be written centered, in 12pt boldface Roman, 12pt below the title.

3.3 Affiliation

Author's affiliation should be written centered, in 11pt Roman, 12pt below the list of authors. A 12pt space should separate two different affiliations.

3.4 Key words

Please, write no more than six key words. They should be written left aligned, in 12pt Roman, and the line must begin with the words **Key words:** boldfaced. A 12pt space should separate the key words from the affiliations.

3.5 Summary (optional)

Use 12pt Italic Roman for the summary. The word **Summary** must be set in boldface, not italicized, at the beginning of the first line. The text should be justified and separated 12pt from the key words, as shown in the first page of these instructions.

4 HEADINGS

4.1 Main headings

The main headings should be written left aligned, in 12pt, boldface and all capital Roman letters. There should be a 12pt space before and 6pt after the main headings.

4.2 Secondary headings

Secondary headings should be written left aligned, 12 pt, boldface Roman, with an initial capital for first word only. There should be a 12pt space before and 6pt after the secondary headings.

5 EDITORIAL HEADING

The first page has to include the Editorial Heading, as shown in the first page of these instructions. Successive pages will include the name of the authors.

6 TEXT

The normal text should be written single-spaced, justified, using 12pt (Times New) Roman in one column. The first line of each paragraph must be indented 0.5cm. There is not inter-paragraph spacing.

7 PAGE NUMBERS

In order to organize the Full Paper, it is better to number the pages. Page numbers are not included in the printing box.

8 FIGURES

All figures should be numbered consecutively and captioned. The caption title should be written centered, in 10pt Roman, with upper and lower case letters.

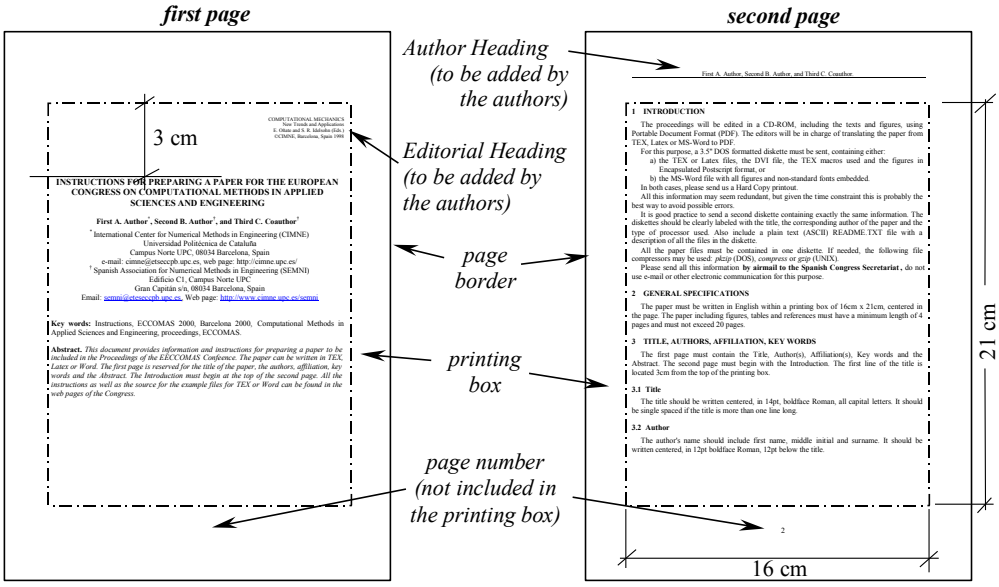

Figure 1: Page layout

A 6pt space should separate the figure from the caption, and a 12pt space should separate the upper part of the figure and the bottom of the caption from the surrounding text.

Figures may be included in the text or added at the bottom of the Full Paper.

9 EQUATIONS

A displayed equation is numbered, using Arabic numbers in parentheses. It should be centered, leaving a 6pt space above and below to separate it from the surrounding text.

The following example is a single line equation:

$$Ax = b \tag{1}$$

The next example is a multi-line equation:

$$Ax = b \tag{2}$$

10 TABLES

All tables should be numbered consecutively and captioned, the caption should be 10pt Roman, upper and lower case letters.

Table 1: Example of the construction of one table

C11	C12	C13
C21	C22	C23
C31	C32	C33
C41	C42	C43
C51	C52	C53

A 6pt space should separate the table from the caption, and a 12pt space should separate

the table from the surrounding text.

11 FORMAT OF REFERENCES

References should be quoted in the text by superscript numbers [1,2] and grouped together at the end of the Full Paper in numerical order as shown in these instructions.

12 CONCLUSIONS

- Full Papers in format for publication should be submitted electronically via the web page of the Conference, before May 26, 2017. The file must be converted to Portable Document Format (PDF) before submission. The maximum size of the file is 4 Mb.
- The speaker (corresponding author) is expected to pay his registration fee during the advance period (before May 26, 2017) for the presentation to be included in the final program of the Conference.

REFERENCES

[1] Zienkiewicz, O.C. and Taylor, R.L. *The finite element method*. McGraw Hill, Vol. I., (1989), Vol. II, (1991).

[2] Idelsohn, S.R. and Oñate, E. Finite element and finite volumes. Two good friends. *Int. J. Num. Meth. Engng* (1994) **37**:3323-3341.